Measurement of group delay of dispersive mirrors with white-light interferometer

Tatiana V. Amotchkina,[1,*] Alexander V. Tikhonravov,[1] Michael K. Trubetskov,[1] Dirk Grupe,[2] Alexander Apolonski,[2,3] and Vladimir Pervak[2]

[1]Research Computing Center, Moscow State University, Leninskie Gory, 119992, Moscow, Russia

[2]Ludwig-Maximilians-Universität München, Am Coulombwall 1, D-85748 Garching, Germany

[3]Institute of Automation and Electrometry, RAS, 630090 Novosibirsk, Russia

*Corresponding author: tatiana@srcc.msu.ru

Received 13 October 2008; revised 26 December 2008; accepted 7 January 2009; posted 8 January 2009 (Doc. ID 102698); published 4 February 2009

A new model for the determination of group delay (GD) and GD dispersion of dispersive mirrors is presented. The algorithm based on this model enables one to process interferometric data provided by a white-light interferometer and to obtain GD wavelength dependence over a broad spectral range. © 2009 Optical Society of America

OCIS codes: 120.5050, 320.7100, 320.7090.

1. Introduction

Optical systems may contain a series of various dispersive optical elements such as mirrors, polarizers, a beam splitter, and lenses. A short pulse propagating through such dispersive optical elements can be distorted, because different spectral components of this pulse accumulate different phases [1].

An important characteristic of a dispersive optical element is group delay (GD) of an optical element, which is defined as the derivative of the spectral phase with respect to the light frequency ω with a minus sign. Group delay dispersion (GDD) is the derivative of GD with respect to ω. In order to properly compensate the phase distortion of an optical pulse, special multilayer coatings can be used [2]. These coatings, called dispersive (or chirped) mirrors, provide high reflection and specific GD and GDD wavelength dependencies in required spectral ranges [3–8]. Modern laser techniques, including femtosecond laser oscillators [6] and external enhancement cavities [8], require a few fs^2 accuracy of GDD determination that is not achievable with the existing approaches.

For decades a number of dispersion measurement devices, including white-light interferometers (WLIs) were reported [9–12]. WLIs are a powerful tool for measuring the GD wavelength dependence of optical elements in a broad spectral range [9,10]. Usually the WLI is a Michelson-type interferometer with a broadband light source [9–11,13,14]. A typical measurement scheme is as follows. An optical element under investigation is placed in the sample arm of the interferometer while the reference arm contains a reference sample with known dispersion. In the course of the measurement process, the reference sample is moved by a motor, and the length of the reference arm is varied. When the reference sample is moved, a spectral intensity distribution (spectral scan) at each motor step position is monitored and recorded. When all scans are recorded, the intensity values can be arranged by the wavelength. A temporal intensity distribution corresponding to a certain wavelength is called an interferogram. GD at each wavelength can be obtained as an instant corresponding to a center position of the interferogram [9,10]. An obvious advantage of this measurement scheme is that it enables one to

0003-6935/09/050949-08$15.00/0

obtain GD simultaneously for all wavelength values generated by a white-light source.

Intensity values in measured interferograms are affected by a noise of the light source and by a noise of the detector. Evidently, determination of center positions from noisy interferograms is not a straightforward task. The problem of extracting GD from interferometric measurements has been considered in several works [9–11,13,14]. The most widely used approach is the Fourier transform technique [11,13,14]. Results provided by the Fourier transform technique are, however, strongly dependent on the noise in interferometric data. In the case of nonuniform motion of a stepper motor, the Fourier transform technique may fail entirely. Correct processing of data requires the application of preliminary smoothing procedures, which significantly decreases wavelength resolution of obtained GD and GDD wavelength dependencies (see Section 5).

In this paper we present a recently developed version of WLI, providing interferometric data and a new algorithm that allows us to perform accurate evaluation of the GD and GDD of dispersive mirrors. In Section 2 we describe in detail our interferometer and the interferometric data that can be obtained using this device. In Section 3 we propose a new model for the interferogram description and present a new algorithm for interferometric data processing. The model and algorithm are aimed at overcoming the instability of interferometric data processing in the case of noisy measurement data. A special part of the algorithm allows us to solve problems caused by nonuniformity of a stepper motor motion. As a result the new algorithm enables us to evaluate the GD and GDD with high accuracy in the spectral range from 600 to 1100 nm. This range is determined not by the algorithm itself, but by hardware components: light sources, detectors, and beam splitter (see Section 2). In Section 3 we also verify the proposed algorithm using computationally simulated interferometric data and estimate an accuracy of GD and GDD evaluation that can be achieved by this algorithm. In Section 4 we apply the new algorithm to processing simulated experimental data. An example of processing of real experimental data is described in Section 5, where we also compare obtained results with the results based on the Fourier transform technique. This comparison clearly illustrates a high wavelength resolution of the developed method.

2. Experimental Setup and Initial Interferometric Data

A schematic of our WLI is presented in Fig. 1. The wavelength grid consists of 1340 spectral points. A fiber-transmitted white light is passed into the interferometer. The incoming collimated beam is divided by a beam splitter cube into two interferometer arms: sample and reference. The reference arm is moved by a stepper motor that drives a precision linear translation stage.

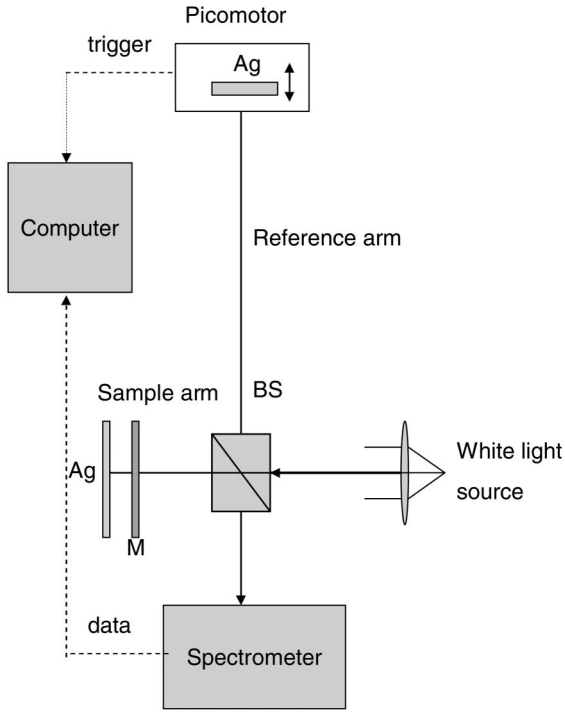

Fig. 1. Schematic of the WLI. BS, beam splitter; Ag, silver mirror; M, dispersive mirror under investigation.

Our motor makes 25 steps per second with a step size of 20–30 nm. A total scanning time is approximately 8 min. During this time interval, we collect 12,000 spectral scans. The exposure time of the CCD camera is less than the interval between adjacent motor steps. All elements of our WLI are placed on a high-quality optical table, reducing vibrations to an acceptable level.

A dispersive mirror is inserted into the sample arm. The beam in the reference arm is reflected back by a silver mirror. A silver mirror was chosen because it has a high reflectivity and negligible dispersion over visible and near infrared spectral ranges. For measurements in the UV range, aluminum mirrors instead of silver mirrors can be used. The beam in the sample arm is reflected back by the dispersive mirror. When two beams overlap, one observes the interference fringe pattern of the spectrum. An example of such fringe with removed background signal is shown in Fig. 2. A contrast of fringes depends on the overlap of the sample and reference beams, on the delay between two arms, and on the reflectivity and wavefront distortion of a sample mirror. The maximum contrast is achieved when two beams overlap completely. This is achieved by adjusting of the end silver mirror in the sample arm.

The overlapped beams are passed by another fiber to a grating spectrometer with CCD cameras. To cover a wide wavelength range, we can use two CCD cameras and two light sources. One CCD camera works in the range of 200–1100 nm, while another one covers the range from 900 to 2200 nm. The second camera is cooled by liquid nitrogen. Two light

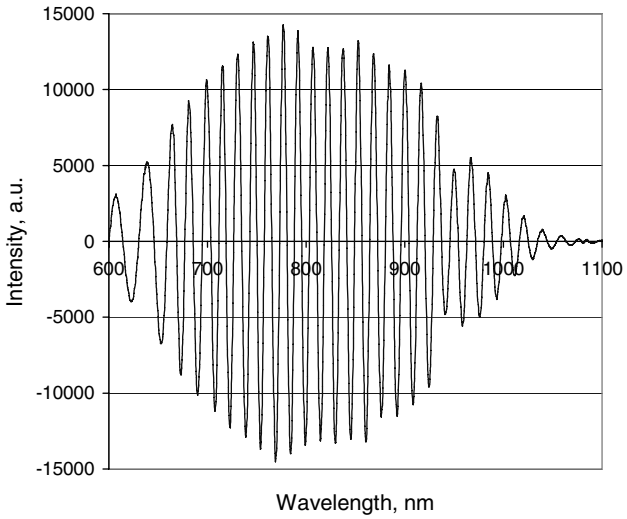

Fig. 2. Typical spectral scan with removed background spectrum.

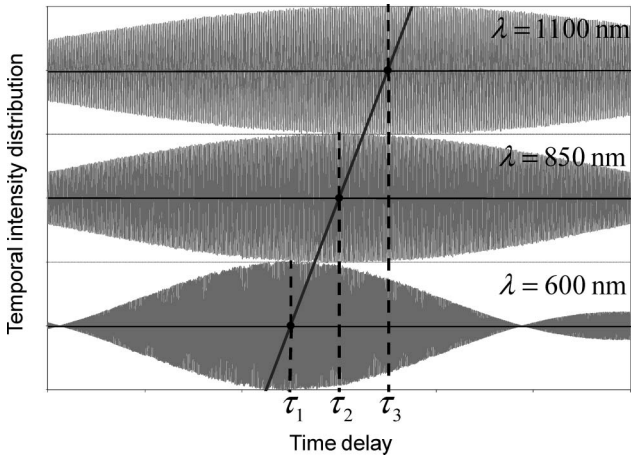

Fig. 3. Interferograms corresponding to three different wavelength values. Coordinates τ_1, τ_2, and τ_3 of the interferograms maxima are indicated by dashed lines. Relative shifts of these coordinates are specified by GDs at respective wavelength values.

sources are a xenon lamp (200–800 nm) and a halogen lamp (350–2200 nm).

A computer is used to store data from the spectrometer. One spectral scan is taken at every step of the motor that moves the silver mirror at the end of reference arm. As mentioned earlier, the stepper motor makes 12,000 steps. The background spectral intensity distribution, i.e., the intensity distribution without interference fringes, is stored and subtracted from all spectral scans. To obtain the background spectral intensity distribution, one manually translates the motorized stage until fringes disappear completely.

As a result of the described measurement process, a two-dimensional array of data containing 1340 × 12,000 points is obtained and stored (for the spectral region 600–1100 nm). Each row of this array contains a spectral scan, and each column contains an interferogram. The level of errors in intensity values caused by light-source noise and detector noise can be estimated at 3%. Typical interferograms corresponding to three different wavelengths values are shown in Fig. 3 by black, light gray, and dark gray curves. If there is no dispersive mirror in the sample arm of the interferometer, then center positions of all interferograms correspond to the same time instant. If a dispersive mirror is placed into the sample arm, then center positions of interferograms are shifted because of the presence of a GD. This fact is demonstrated in Fig. 3.

It worth mentioning the main reason for using large arrays of experimental data in our method. In principle, phase spectral dependence can be obtained with the help of spectral interferometry using a single spectral measurement. As an example, Kumar and Rao [15] used the information provided by a single spectral measurement for a precise determination of the refractive index of dispersive medium placed in one of the arms of a Michelson interferometer. We, however, are interested not in a spectral phase itself but in a spectral dependence of GDD, which is a second derivative of the phase with respect to frequency ω.

To obtain GDD spectral dependence, having in hand experimental phase data, one ought to perform a numerical differentiation of this phase. It is known from the mathematical theory of ill-posed problems [16] that in the presence of experimental errors, numerical differentiation is a highly unstable operation. As a result, numerical differentiation may give entirely wrong results even for GD spectral dependence. Obtaining correct GDD spectral dependence requires differentiating experimental phase data two times, and this is a much more problematic operation.

To overcome problems connected with experimental data processing, the mathematical theory proposes to take into account more experimental information [16]. Using two-dimensional arrays of interferometric data is a productive approach to an accurate determination of GD spectral dependence. This was demonstrated in Ref. [17], where spectrally resolved white-light interferometry was used for such a determination. In our approach, we use classical interferometer arrangement with a movable mirror to obtain two-dimensional arrays of interferometric data. As mentioned earlier, the total measurement time is approximately 8 min, which is not too much. With the power of modern personal computers, processing large arrays of experimental data is not a problem from the point of view of computational time. The main problem is developing a mathematical algorithm for data processing that can provide reliable GDD spectral dependence. This issue is addressed in Section 3.

3. Model Interferograms and Algorithm for Data Processing

A. Model Interferograms

As indicated in Section 2, each interferogram represents intensity values corresponding to one of the wavelength values and 12,000 positions of the

movable mirror in the reference arm. It is commonly accepted to plot an interferogram versus a time axis with the time calculated as a delay of the wave packet propagating in the reference arm. We assign $t = 0$ to the first position of the movable mirror. Other coordinates on the time axis are calculated as follows:

$$t_i = \sum_{k=1}^{i-1} \Delta t_k, \qquad \Delta t_k = 2\Delta s_k / c, \tag{1}$$

where i is the respective number of the motor step position, Δs_k is the distance between positions of the motor at the kth and $(k+1)$th steps, Δt_k is the time increment of wave propagation caused by changing a motor position between the kth and the $(k+1)$th steps, and c is light velocity in a vacuum.

Equation (1) reflects a real situation in which distances between adjacent motor positions are not all the same. Our algorithm of interferogram data processing requires knowing t_i values with sufficient accuracy. The algorithm for calculating t_i is described in Subsection 3.C.

Intensity values represented by interferograms correspond to quasi-monochromatic wave packets with a central wavelength specified by the used CCD camera. To write down an interferogram model, we assume that each wave packet has a rectangular spectrum with a central wavelength λ and a spectral width $\Delta\lambda$. In this case, in the absence of a sample mirror, an interferogram is represented by the model equation (see, for example, Ref. [18]):

$$I(t) = \frac{1}{2} I\gamma(t) \cos \omega t, \qquad \omega = \frac{2\pi c}{\lambda}, \tag{2}$$

where I is the intensity of the wave packet, c is the light velocity, and $\gamma(t)$ is the envelope function specified by

$$\gamma(t) = \frac{\sin(\Delta\omega t/2)}{\Delta\omega t/2}, \qquad \Delta\omega = \frac{4\pi\Delta\lambda}{\lambda^2 - \Delta\lambda^2}. \tag{3}$$

When a dispersive mirror is inserted in the sample arm, Eq. (2) is modified due to a GD caused by a dispersive mirror and takes the form [18]

$$I(t) = \frac{1}{2} I\gamma(t - \tau(\lambda)) \cos(\omega t + \alpha(\tau)), \qquad \omega = \frac{2\pi c}{\lambda}. \tag{4}$$

Here $\tau(\lambda)$ is a GD at a given wavelength λ, and α is an additional phase term dependent on a GD. It will be seen that this phase term is not essential for our algorithm of data processing. For this reason, we do not discuss it in more detail.

It is seen from Eq. (4) that, in the presence of a dispersive mirror, a center position of an interferogram corresponds to $t = \tau(\lambda)$. Our algorithm for calculating a GD is based on this fact. It is discussed in Subsection 3.B.

B. Data Processing Algorithm

Consider an interferogram corresponding to a wavelength λ_j. Denote I_i intensity values corresponding to time coordinates t_i. Recall that each interferogram has 12,000 such values forming an oscillating pattern versus the time axis. Our algorithm employs not all I_i values, but only local minima $I_{\min,k}$ and local maxima $I_{\max,k}$ of an interferogram pattern. The introduction of these local minima and maxima is shown in Fig. 4.

Let $N_{\max}$ and $N_{\min}$ be total numbers of local maxima and minima of an interferogram. In our experiments, typical values of these numbers are 350–400. Local extrema of an interferogram form an envelope of this interferogram. It is natural to assume that the center position of the envelope at the wavelength λ_j corresponds to GD $\tau(\lambda_j)$.

In order to find a center position of an envelope, we introduce a model envelope function $I_{\text{env}}(t)$:

$$I_{\text{env}}(t) = \frac{1}{2} I \frac{\sin(\Delta\omega(t-\tau)/2)}{\Delta\omega(t-\tau)/2}, \qquad \Delta\omega = \frac{4\pi\Delta\lambda}{\lambda^2 - \Delta\lambda^2}. \tag{5}$$

This model envelope function, $I_{\text{env}}(t)$, is obtained from Eq. (4) for the model interferogram $I(t)$ by omitting the cosine term. For each wavelength λ_j, the envelope function is specified by three model parameters, I, $\Delta\lambda$, and τ, that may be different for different wavelength values λ_j. The introduction of two additional parameters along with GD τ is connected with the fact that the intensity and the spectral width of the quasi-monochromatic wave packet are not known and are dependent on wavelength λ_j.

We estimate the closeness between the model envelope function $I_{\text{env}}(t)$ and measured intensity local extrema $I_{\max,k}$ and $I_{\min,k}$ by the discrepancy function (DF):

$$\text{DF} = \sum_{k=1}^{N_{\max}} (|I_{\text{env}}(t_{\max,k})| - I_{\max,k})^2 + \sum_{k=1}^{N_{\min}} (|I_{\text{env}}(t_{\min,k})| + I_{\min,k})^2. \tag{6}$$

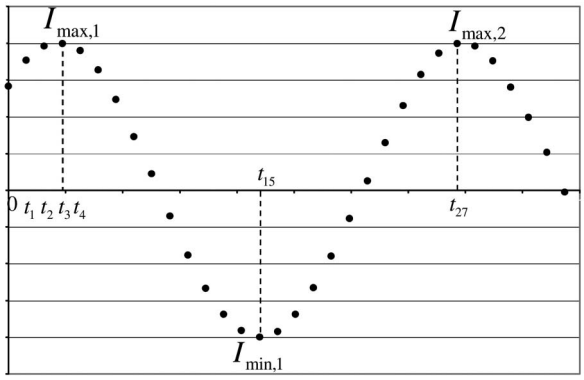

Fig. 4. Introduction of local minima and local maxima of an interferogram.

In Eq. (6), $t_{\max,k}$ and $t_{\min,k}$ are coordinates of the local intensity maxima and minima. These coordinates are calculated at the preliminary data processing step described here.

Our algorithm is based on the minimization of the DF with respect to the three model parameters. For each wavelength λ_j, parameters providing the best fit of measured local extrema are found. The found value of the parameter τ represents the GD at wavelength λ_j. A typical fitting of measured local extrema by the model envelope function is shown in Fig. 5, which corresponds to the wavelength of 932 nm. The found parameter values are $I = 4540.5$ a.u., $\Delta\lambda = 2.38$ nm, and $\tau = 518.55$ fs.

Calculating parameter τ for all interferograms, we obtain the GD wavelength dependence $\tau(\lambda_j)$ over the whole set of wavelength values $\lambda_j, j = 1, \ldots, 1340$. Because of errors in experimental intensity values, dependence $\tau(\lambda_j)$ also contains some errors, and a straightforward numerical differentiation of dependence $\tau(\lambda)$ results in a set of noisy values that has nothing in common with GDD(λ). For this reason, a special procedure for smoothing the found GD wavelength dependence is required. In our algorithm, we use a standard procedure based on the approximation of the obtained $\tau(\lambda)$ dependence by smoothing cubic splines [19]. As a result of such approximation, we obtain a smooth twice-differentiable dependence $\tau(\lambda)$. The corresponding GDD(λ) is obtained by differentiation of this function:

$$\mathrm{GDD}(\lambda) = -\frac{\lambda^2}{2\pi c} \cdot \frac{\mathrm{d}\tau(\lambda)}{\mathrm{d}\lambda}. \tag{7}$$

C. Calculating Coordinates of the Time Axis

Unfortunately, steps of the motor in the reference arm in the interferometer are not exactly the same. For this reason, coordinates on the time axis corresponding to the motor step positions are not evenly distributed and cannot be calculated based on the averaged time increment Δt_{av}, which is approximately 0.15 – 0.2 fs. Our algorithm requires knowing not an average time increment but actual time increments, $\Delta t_1, \ldots, \Delta t_{N-1}$, between time coordinates corresponding to all motor step positions (N is the number of motor steps). Here we present a procedure for calculating these time increments with sufficient accuracy.

Consider the interferogram I_i, $i = 1, \ldots, N$, corresponding to wavelength λ_0. A typical fragment of this interferogram is schematically shown in Fig. 6. Measured intensity values are marked by circles. We assume that these values are close to the analytical intensity $I(t)$ values presented by Eq. (4). On a small segment of the time axis, this analytical intensity is a trigonometric periodic function with the period T equal to λ_0/c. This periodic function is shown in Fig. 6 by a dotted curve. Points ξ_l and ξ_r in Fig. 6 indicate the boundaries of a semiperiod of $I(t)$.

We subdivide the time axis into time intervals corresponding to all semiperiods of $I(t)$. Let us denote K as the total number of these semiperiods and p as a current number of a semiperiod. We further assume that, inside each semiperiod, all time increments are equal. The time increment for the semiperiod p is denoted as δ_p. Note that, for different semiperiods δ_p, values may be different.

Consider a semiperiod with the number p. Let $I_{p,2}, \ldots, I_{p,k-1}$ be intensity values corresponding to time coordinates that lie inside the time interval of this semiperiod (see Fig. 6). The intensity value corresponding to the first time coordinate located to the left of ξ_l is denoted as $I_{p,1}$, and the intensity value corresponding to the first time coordinate located to the right of ξ_r is denoted as $I_{p,k}$.

The number of full time increments δ_p inside the time interval $[\xi_l, \xi_r]$ is equal to $K - 3$. There are also two fractions of δ_p at the beginning and at the end of this interval, $\delta_{p,1}$ and $\delta_{p,2}$ (see Fig. 6). Assuming linear $I(t)$ dependencies between the first two and last two points, we find that

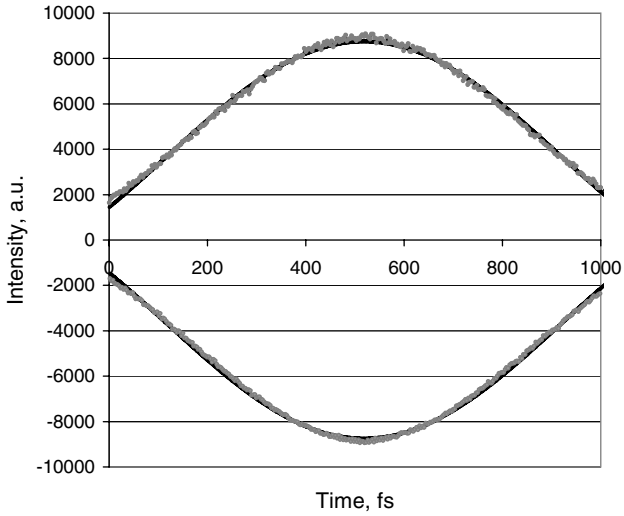

Fig. 5. Typical fitting of local extrema of the measured interferogram (gray circles) by the model envelope function defined by Eq. (5) (solid black curve).

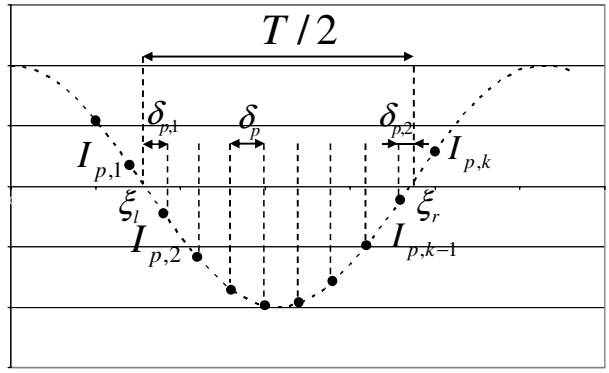

Fig. 6. Schematic illustrating the procedure of calculating time increments.

$$\delta_{p,1} = \frac{I_{p,1}\delta_p}{I_{p,2} - I_{p,1}}, \qquad \delta_{p,2} = \frac{I_{p,k}\delta_p}{I_{p,k} - I_{p,k-1}}. \tag{8}$$

The time interval between the ξ_l and ξ_r points can be now expressed as

$$\xi_r - \xi_l = (K-3)\delta_p + \delta_{p,1} + \delta_{p,2}. \tag{9}$$

On the other hand, $\xi_r - \xi_l$ is equal to $T/2$, and we derive from Eq. (9) that

$$\delta_p = \frac{1}{2}T\left[K + \frac{I_{p,2}}{I_{p,2} - I_{p,1}} + \frac{I_{p,k}}{I_{p,k} - I_{p,k-1}}\right]^{-1}. \tag{10}$$

Equation (10) is used for calculating the δ_p values for all semiperiods one by one. As a result, we obtain estimations for all time increments $\Delta t_1, \ldots, \Delta t_{N-1}$. The described procedure used a single interferogram to estimate all time increments. It is natural to check whether interferograms corresponding to different wavelength values will give close estimations for increment values. If so, then this will approve the validity of the applied procedure. In Fig. 7, we present typical time increments calculated from interferograms corresponding to the wavelength values of 750, 830, and 910 nm. One can see that there is an excellent agreement between the obtained results.

4. Application of the Algorithm for Simulated Data Processing and Estimation of the Accuracy of Group Delay and Group Delay Dispersion Calculation

In order to verify the proposed algorithm, we applied it for processing simulated interferometric data. In these experiments, we used simulated data that are qualitatively similar to experimental interferometric data. In order to simulate noisy intensity values I_i, we introduce relative errors δ_i to the model intensity values $I(t_i)$ calculated using Eq. (4):

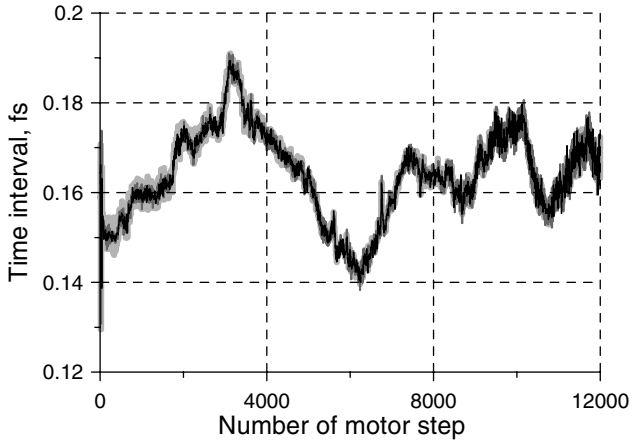

Fig. 7. Time increments caused by changing the motor position. Black narrow curve, increments corresponding to the wavelengths of 750 nm; gray medium-width curve, 830 nm; light gray wide curve, 910 nm.

$$I_i = I(t_i)(1 + \delta_i), \qquad i = 1, \ldots, N, \tag{11}$$

where N is the number of motor steps.

We assume that errors in intensity data δ_i are random errors distributed by the normal law with mean values equal to zero and standard deviations equal to σ. We refer to σ as the level of errors in the intensity values. For the sake of simplicity, we consider here only the case when σ does not depend on the wavelength λ_j.

It is mentioned in Section 2 that the level of errors in experimental data is estimated at 3%. Estimation of standard deviation of time increments based on the results of Subsection 3.C gives that it is of approximately 7% of the average time increment value. In our experiments, we simulated intensity values with the error level σ equal to 1%, 3%, and 5%, average time increment equal to 0.2 fs, and standard deviation of time increment fluctuations equal to 0.014 fs.

Experimental data show that the interferograms corresponding to higher wavelength values are wider than those corresponding to shorter wavelengths (see Fig. 3). Evidently a width of an interferogram affects the accuracy of GD calculation, because for wider interferograms, it is more difficult to find their center positions. As a consequence, the accuracy of GD calculations at the upper boundary of the spectrum is worse than the accuracy in the middle and left boundary of the spectrum. A width of interferogram is defined by the value $\Delta\omega$ that is expressed through $\Delta\lambda$ and λ [see Eqs. (2) and (3)]. To simulate data similar to experimental data, we specified the dependence $\Delta\lambda(\lambda) = A + B/(C - \lambda)$ with values $A = 1.128$, $B = 83.52$, and $C = 1226$. Parameters A, B, and C were determined for one of the samples and are typical for most cases.

In the course of algorithm verification, we processed simulated data with various types of dispersive mirror GD dependencies. Here we present results of processing simulated data that correspond to a 49-layer dispersive mirror with a high reflection in the spectral range from 700 to 900 nm and analytical GD and GDD dependencies shown in Fig. 8 by dashed gray curves. The determined GD and GDD dependencies in the case of 3% errors in intensity values are shown in Fig. 8 by black curves. One can observe a good agreement between the simulated and determined GD and GDD dependencies. To provide numerical estimations of an accuracy of data processing in the case of different errors in simulated data, we consider standard deviations σ_{GD} and σ_{GDD} between simulated and calculated dependencies. These standard deviations are defined by

$$\sigma_{\mathrm{GD}} = \sqrt{\frac{1}{M}\sum_{j=1}^{M}(\tau(\lambda_j) - \tau_S(\lambda_j))^2},$$
$$\sigma_{\mathrm{GDD}} = \sqrt{\frac{1}{M}\sum_{j=1}^{M}(\mathrm{GDD}(\lambda_j) - \mathrm{GDD}_S(\lambda_j))^2}, \tag{12}$$

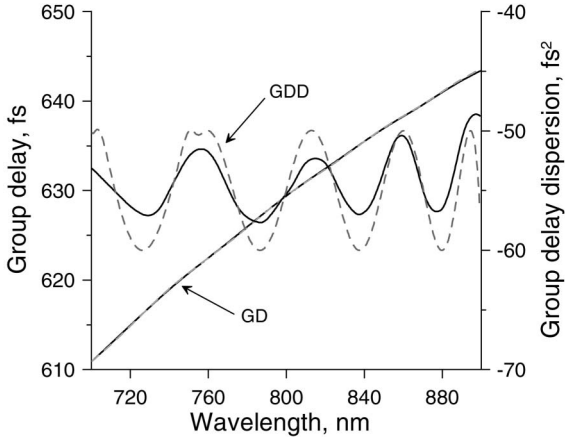

Fig. 8. Comparison of analytical GD and GDD wavelength dependencies (dashed gray curves) and calculated GD and GDD wavelength dependencies (black curves).

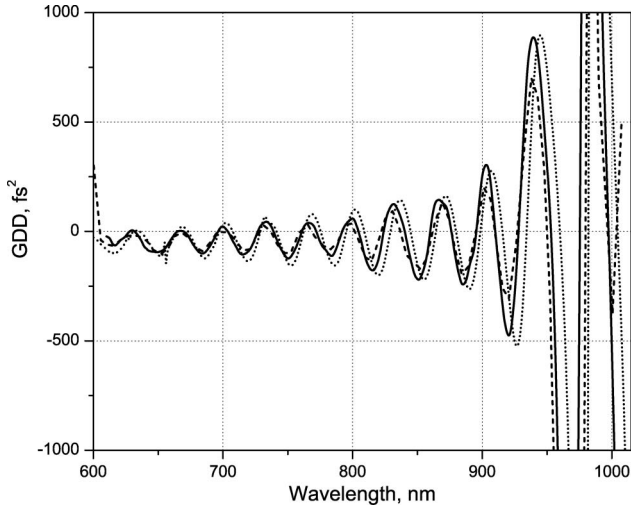

Fig. 9. GDD obtained from the experimental data by two different methods: Fourier transform technique (dashed curve) and new algorithm described in this paper (solid curve). Theoretical GDD dependence of this mirror is shown by dotted curve for comparison.

where $\tau_S(\lambda_j)$ and $\mathrm{GDD}_S(\lambda_j)$ are initial GD and GDD data, and $\tau(\lambda_j)$ and $\mathrm{GDD}(\lambda_j)$ are calculated GD and GDD dependencies. In Table 1, we compare σ_{GD} and σ_{GDD} values in the cases of 1%, 3%, and 5% errors in simulated data. These values of σ_{GD} and σ_{GDD} are typical for experiments with other simulated GD dependencies as well. As mentioned earlier, our experimental interferograms have an accuracy of 3%. Thus based on the results of simulated data processing, we can expect a relative accuracy of GD calculations of approximately 0.3% and a relative accuracy of GDD calculation of approximately 4%. We determined relative accuracy of GD determination as a ratio σ_{GD} to typical GD variation in the considered wavelength range. For GDD, the relative accuracy is determined as a ratio of σ_{GDD} to a maximum of |GDD|.

5. Application of the Algorithm to Experimental Data Processing

Here we present results of the application of the novel algorithm for experimental data processing. We consider a broadband dispersive mirror designed and manufactured for the wavelength range from 550 to 1050 nm for generating sub-5 fs mJ-level pulses behind the hollow gas-filled fiber in a kilohertz Ti:Sa laser system.

In Fig. 9, we present GDD obtained with the help of the Fourier transform technique (dotted curve) and GDD obtained by the described algorithm (solid curve). First, one can see that the difference increases toward the IR part of spectrum and reaches values of 100 fs^2. Second, one can conclude that the Fourier transform technique provides a GDD wavelength dependence that is significantly oversmoothed. It happens because the Fourier transform technique requires one to preprocess the data provided by the so-called binning procedure that removes essential information from interferograms.

Our CCD camera provides measurement data at 1340 wavelength points. The binning procedure takes measurement data at 15 adjacent points and averages data over these points. Thus the binning procedure reduces spectral data to approximately 100 wavelength points. As a result, the estimated wavelength resolution of the Fourier transform technique is approximately 5 nm.

Without preprocessing by the binning procedure, the Fourier transform technique is not able to perform data evaluation. This is equivalent to a poor wavelength resolution of the Fourier transform technique as compared to the new algorithm. Our novel algorithm provides a more detailed GDD wavelength dependence, because during data processing, we take into account all information from the WLI. In Fig. 9, we also present a theoretical GDD of this mirror (dashed curve). It is clearly seen that novel approach of WLI data processing provides results much closer to the theoretical GDD wavelength dependence. Extremal values of the GDD are very close, and some shift of the obtained GDD dependence from the theoretical one is clearly attributed to the presence of systematic errors in layer thicknesses of the deposited mirror.

The obtained GD and GDD wavelength dependencies can be used for the postproduction characterization of broadband dispersive mirrors [4]. Using these dependencies along with spectrophotometric measurements allows one to investigate reasons causing deviations of measured GD and GDD dependencies from the expected ones. This allows one to perform corrections of the manufacturing process in order to increase a quality of production.

Table 1. Effect of Error Level in Simulated Data on the Accuracy of Group Delay and Group Delay Dispersion Calculation

Error Level σ in Simulated Data (%)	1	3	5
Accuracy of GD Calculation, σ_{GD} (fs)	0.05	0.1	0.2
Accuracy of GDD Calculation, σ_{GDD} (fs^2)	1.5	2	3

6. Conclusions

We presented a new technique for determining GD and GDD of dispersive mirrors. The evaluation procedure consists of two main steps: measurement of interferometric data and processing of these data. Experimental data are provided by a WLI. Data processing is performed using a new algorithm described in this paper. The proposed algorithm explores all available experimental data and, due to this fact, allows one to reliably determine GD and GDD dependencies in the case of noisy experimental data and nonuniform motor motion.

The accuracy of results is estimated in the paper based on processing simulated data. It is shown that the expected accuracy of GD and GDD evaluation is approximately 0.3% and 4%, respectively. This accuracy is sufficient for most applications using femtosecond dispersive optics. Future experiments with femtosecond enhancement cavities will require even higher GDD accuracy (better than 1%). This level of accuracy can be achieved by a further improvement of the stepping motor and the detection system of our measurement setup.

The authors are very grateful to F. Krausz for the attention to this work and the fruitful discussions.

This work was supported by the Deutsche Forschungsgemeinschaft (DFG) Cluster of Excellence Munich Centre for Advanced Photonics (www.munich-photonics.de) and the Russian Fund of Basic Research (RFBR), project 07-00140a (www.rfbr.ru).

References

1. J.-C. Diels and W. Rudolph, *Ultrashort Laser Pulse Phenomena*, 2nd ed. (Academic, 2006).
2. R. Szipöcs, K. Ferencz, C. Spielmann, and F. Krausz, "Chirped multilayer coatings for broadband dispersion control in femtosecond lasers," Opt. Lett. **19**, 201–203 (1994).
3. V. Pervak, A. V. Tikhonravov, M. K. Trubetskov, S. Naumov, F. Krausz, and A. Apolonski, "1.5-octave chirped mirror for pulse compression down to sub-3 fs," Appl. Phys. B **87**, 5–12 (2007).
4. A. V. Tikhonravov, M. K. Trubetskov, V. Pervak, F. Krausz, and A. Apolonski, "Design, fabrication and reverse engineering of broad band chirped mirrors," in *Proceedings, Optical Interference Coatings on CD-ROM, Presentation WB4*, Tucson, Arizona (OSA, 2007).
5. V. Pervak, C. Tiesset, A. Sugita, S. Naumov, F. Krausz, and A. Apolonski, "High-dispersive mirrors for femtosecond lasers," Opt. Express **16**, 10220–10233 (2008).
6. V. Pervak, S. Naumov, F. Krausz, and A. Apolonski, "Chirped mirrors with low dispersion ripple," Opt. Express **15**, 13768–13772 (2007).
7. V. Pervak, F. Krausz, and A. Apolonski, "Dispersion control over the UV-VIS-NIR spectral range with HfO_2/SiO_2 chirped dielectric multilayers," Opt. Lett. **32**, 1183–1185 (2007).
8. A. Ozawa, J. Rauschenberger, C. Gohle, M. Herrmann, D. R. Walker, V. Pervak, A. Fernandez, R. Graf, A. Apolonski, R. Holzwarth, F. Krausz, T. W. Haensch, and T. Udem, "High harmonic frequency comb for high resolution spectroscopy," Phys. Rev. Lett. **100**, 253901 (2008).
9. W. H. Knox, N. M. Pearson, K. D. Li, and C. A. Hirlimann, "Interferometric measurements of femtosecond group delay in optical components," Opt. Lett. **13**, 574–576 (1988).
10. W. H. Knox, "Dispersion measurements for femtosecond-pulse generation and applications," Appl. Phys. B **58**, 225–235 (1994).
11. A. Gosteva, M. Haiml, R. Paschotta, and U. Keller, "Noise-related resolution limit of dispersion measurements with white-light interferometers," J. Opt. Soc. Am. B **22**, 1868–1874 (2005).
12. M. Beck and I. A. Walmsley, "Measurement of group delay with high temporal and spectral resolution," Opt. Lett. **15**, 492–494 (1990).
13. K. Naganuma, K. Mogi, and H. Yamada, "Group-delay measurement using the Fourier transform of an interferometric cross correlation generated by white light," Opt. Lett. **15**, 393–395 (1990).
14. S. Daddams and J.-C. Diels, "Dispersion measurements with white-light interferometry," J. Opt. Soc. Am. B **13**, 1120–1129 (1996).
15. V. N. Kumar and D. N. Rao, "Using interference in the frequency domain for precise determination of thickness and refractive indices of normal dispersive materials," J. Opt. Soc. Am. B **12**, 1559–1563 (1995).
16. A. N. Tikhonov and V. Y. Arsenin, *Solutions of Ill-Posed Problems* (Wiley, 1977).
17. A. P. Kovács, K. Osvay, Z. Bor, and R. Szipöcs, "Group-delay measurement on laser mirrors by spectrally resolved white-light interferometry," Opt. Lett. **20**, 788–790 (1995).
18. S. A. Akhomanov and S. Y. Nikitin, *Physical Optics* (Oxford University, 1997).
19. C. H. Reinsch, "Smoothing by spline function," Numer. Math. **10**, 177–183 (1967).